Study of novel flow channels influence on the performance of direct methanol fuel cell

Accepted for publication by: International Journal of Hydrogen Energy

Study of novel flow channels influence on the performance of direct methanol fuel cell

Jegathishkumar Ramasamy [a], Karthikeyan Palaniswamy [b,*], Thanarajan Kumaresan [b], Mathan Chandran [b], Rui Chen [c]

[a] Department of Mechanical Engineering, PSG College of Technology, Coimbatore, 641004, India

[b] Department of Automobile Engineering, PSG College of Technology, Coimbatore, 641004, India

[c] Department of Aeronautical and Automotive Engineering, Loughborough University, Loughborough, United Kingdom

Highlights:

- Numerical study on DMFC model with novel flow channel design.
- Comparative study on DMFC performance with serpentine, zigzag and pin flow channels.
- Effect of pressure drop, velocity, oxygen and water concentration on DMFC performance.
- Performance comparison of DMFC with various flow channel design.
- Power enhancement of DMFC by 17.8% using novel flow field design.

Keywords:

Direct methanol fuel cell; Flow parameter effect; Flow field design; Performance improvement; Uniform flow; Under rib convection

Abstract

The existing flow channels like parallel and gird channels have been modified for better fuel distribution in order to boost the performance of direct methanol fuel cell. The main objective of the work is to achieve minimized pressure drop in the flow channel, uniform distribution of methanol, reduced water accumulation, and better oxygen supply. A 3D mathematical model with serpentine channel is simulated for the cell temperature of 80 ^{o}C, 0.5 M methanol concentration. The study resulted in 40 mW/cm^2 of power density and 190 mA/cm^2 of current density at the operating voltage of 0.25 V. Further, the numerical study is carried out for modified flow channels to discuss their merits and demerits on anode and cathode side. The anode serpentine channel is unmatched by the modified zigzag and pin channels by ensuring the better methanol distribution under the ribs and increased the fuel consumption. But the cathode serpentine channel is lacking in water management. The modified channels at anode offered reduced pressure drop, still uniform reactant distribution is found impossible. The modified channels at cathode outperform the serpentine channel by reducing the effect of water accumulation, and uniform oxygen supply. So the serpentine channel is retained for methanol supply, and modified channel is chosen for cathode reactant supply. In comparison to cell with only serpentine channel, the serpentine anode channel combined with cathode zigzag and pin channel enhanced power density by 17.8% and 10.2% respectively. The results revealed that the zigzag and pin channel are very effective in mitigating water accumulation and ensuring better oxygen supply at the cathode.

Nomenclature

Symbols

Cp	Specific heat capacity (J/kg.K)
C	Molar concentration (mol/m^3)
D	Diffusivity (m^2/s)
F	Faraday constant
i	Current density (A/m^2)
K	Permeability (m^2)
k	Thermal conductivity (W/m.K)
N	Molar flux (mol/m^2.s)
P	Pressure (Pa)
R	Gas constant (J/mol.K)
Ru	Universal gas constant (J/mol.K)
S	Source term
T	Temperature (K)
u	Velocity (m/s)
Y	Mass fraction

Greek letters

α	Transfer coefficient
λ	Advection correction factor
δ	Thickness (m)
ε	Porosity
ρ	Density (kg/m^3)
σ	Ionic conductivity (S/m)
μ	Viscosity (N.S/m^2)
φ	Potential (V)
η	Overpotential (V)

Superscript and subscript

a	anode
c	cathode
gdl	gas diffusion layer

eff	effective
acl	anode catalyst layer
mem	membrane
ccl	cathode catalyst layer
l	liquid
g	gas
Pt	platinum
ref	reference
rev	reversible
sat	saturation
xover	cross over

Introduction

The commercialization of direct methanol fuel cell (DMFC) is facing huge challenges like size, complexity in design and expensive catalyst material when compared to conventional battery power sources. Besides, the practical difficulties like poor methanol oxidation reaction (MOR), fuel cross over, Carbon dioxide (CO_2) bubble formation, water and thermal management, sluggish Oxygen reduction reaction (ORR) and massive demand of noble metal hinder the commercialization of DMFC from substituting the conventional batteries [1]. It is reported that, a single cell can produce 48 mW/cm^2 of power density at 0.26 V, 80 °C with 4 M methanol concentration. This power output is sufficient to power portable electronics by stacking multiple cells [2]. In recent days, the DMFC based power sources are commercialized with portable electronic devices by leading manufacturers like Toshiba, Samsung, Panasonic etc., Commercial products such as mobile and computer chargers, material handling equipment, hearing aids are DMFC powered and fuel cell development is gaining more attention. In addition, DMFC is successfully designed to power military base and telecommunication towers in remote areas [3].

In DMFC, the flow channel is responsible for supplying fuel or reactant over the catalyst surface. Alias et al. [4] reviewed different flow channel study carried out by different researchers and listed the advantage of each flow channels considered. This paper also presented different development carried out on Membrane electrode assembly (MEA). Apart from fuel supply, the anode flow field also aids in removal of electrochemical by-product CO_2 from the catalyst surface. The gaseous CO_2 bubble diminishes the overall cell performance by blocking the reactant that is reaching the catalyst surface thereby causing mass transport loss [5]. These CO_2 bubbles have to be removed from the diffusion layer surface as it tends to block the porous volume. Thus, it reduces the methanol flux on the catalyst surface leading to concentration loss of reactants. Increasing the anode flow rate removes the CO_2 bubbles, otherwise resident time of reactant gets reduced, which lessens the electrochemical activity. Increasing fuel supply increases the pumping power significantly. Reducing the anode flow rate is insufficient to remove the bubbles. So, optimizing the flow rate is necessary to optimize the performance of DMFC [6]. Su et al. [7] performed numerical study on single cell DMFC with serpentine sinusoidal corrugated flow channel. The sinusoidal geometry effect is very small on fuel supply but it effectively separated CO_2 bubbles from the wall. Goor et al. [8] revealed that increasing the hydrophobicity of bipolar flow channel reduces gaseous CO_2 accumulation in the flow

path. But it is recommended to reduce the hydrophobicity in the cathode side to prevent water accumulation and reported 28% increased power density. Similarly, the cathode flow field also removes the cross-over methanol and excess water formation from the catalyst. The crossover of methanol happens at low current density region operated at high methanol concentration. Xu et al. [9] presented a new anode fuel supply channel which vaporizes the methanol in the flow channel itself by absorbing the heat generated in the cell. It permits the DMFC to be operated at high methanol concentration up to 16 M. But water management at cathode side is to be managed to prevent the back diffusion of water from cathode to anode. Hsieh et al. [10] experimented DMFC performance with single inlet serpentine flow channel and four outlet channels on anode and cathode side to study water and CO_2 management. The study presented that four outlet flow channel revealed significant performance enhancement by effectively mitigating electrochemical by-products. Many flow channels such as single serpentine, multi serpentine, interdigitated, parallel, grid type, etc., were proposed by many researchers for fuel supply and by-product management. Ramesh et al. [11] performed a transient study in one-dimensional model with interdigitated flow channel for predicting the time taken to attain steady state in an active DMFC. It is reported that the cell delivers steady performance after 45 min only. Park et al. [12] carried out a numerical and experimental study using single serpentine flow channel with different land and rib geometry to predict its influence on the performance of DMFC. The results revealed that 1 mm channel and 0.5 mm rib width showed better performance. The narrow rib width helped in removing water molecules under the rib, which ensured improved convection of air under the rib. It is reported that reducing the channel width increases the fuel diffusion through gas diffusion layer as the flow velocity increases. The fuel supply is more even because of smaller channel width and rib width. And high pressure drop due to smaller channel width increases gas removal capacity [13]. Ouellette et al. [14] studied serpentine, bio-inspired interdigitated flow and non-interdigitated flow channels performance on single cell DMFC. The serpentine and interdigitated flow channels performed better by effectively increasing the fuel supply under the ribs. But the serpentine channel was reported effective because other channel had more dead zones. Yang et al. [15] modelled a 5 cm^2 active cell area to predict the influence of land and channel cross-sectional area on the performance of DMFC. The under rib convection effect is studied for different open ratios. It is found that increasing land area reduces the performance, and decreasing channel cross-sectional area increases the cell performance. As the pressure drop across the channel increases the mass transport mechanism changes from diffusion to convection which increases the cell performance. Turkmen et al. [16] made a statistical relationship study on 25 cm^2 cell by varying the channel width and gap between channels. It is reported that the channel width have significant influence on pressure drop, but the gap between channels have no effect on the pressure drop. Wei Yuan et al. [17] used the visualization method to study two-phase phenomenon of anode side by fabricating a transparent fuel cell. The pressure drop seems to fluctuate during the operation due to the CO_2 bubble behavior. The fluctuation in pressure drop is due to the formation of gas slugs which eventually drains out through the exit. The author experimented cell performance with three different forms of serpentine channels like conventional serpentine, round-cornered serpentine and broad cross-sectional path serpentine. The broad cross-section channel maintained uniform distribution of methanol and highest performance is achieved, followed by the round corner and conventional serpentine. Oliveira et al. [18] experimented performance of DMFC subjected to different operating parameters in three different flow channels such as single-pass serpentine, multi-pass serpentine and parallel serpentine mixed-flow channel. The experimental results revealed that the performance of DMFC is similar for all the serpentine channels taken for study, yet single-pass serpentine at cathode exhibited better performance among all the channels. The multi-pass serpentine channel eases water removal by producing more pressure drop and the performance is reported better when

operated at high methanol concentration. Conversely the mixed flow channel revealed better performance when the cell is operated at low temperature and lower methanol concentration. The multi-serpentine channel has uneven supply of fuel at every turn of flow path due to reduced flow velocity. It causes by-product accumulation at each corner. So current density uniformity is highly affected. But the single serpentine channel has increased current density at each turn due to high flow velocity and reduced by-product accumulation [19]. Hu et al. [20] compared the performance of serpentine channel with non-uniform serpentine channel in which the cross section is reduced from inlet to exit. It resulted in 18% higher power generation by uniform supply of fuel supply. Radwan et al. [21] modified the conventional serpentine for enhancing the convection mass transport under the rib. This modified channel enabled higher mass transport on the catalyst layer compared to a conventional serpentine channel. The flow channel with more paths and lengthy rib enhanced under rib convection and improved the power density by 52.9%. Ouellette et al. [22] done study on influence of cathode flow channel on cell performance using four different flow channels such single serpentine, three serpentine, parallel serpentine and grid channel. It is reported that single serpentine supplied oxygen more evenly and resulted better performance. But the grid channel is failed to deliver oxygen properly because of dead zone inside the flow path. Jung et al. [23] compared the conventional DMFC cell with interdigitated anode fuel supply system. It is reported current density is improved by mitigating non-uniformity of fuel supply. Wei Yuan et al. [24] experimented DMFC with flow channels such as serpentine, parallel and porous channel in anode and cathode to measure the performance of DMFC and to study the influence of different flow channels. It is found that the serpentine flow field in the anode performed better by preventing CO_2 bubble accumulation in the flow path. High anode flow rate is preferred to remove the bubbles from the flow channel. The parallel flow channel in the anode is poorly sensitive to flow rate. The porous channel showed lower performance compared to the other. However, the influence of flow rate seems significant. The performance of DMFC using serpentine flow channel in cathode is insensitive to the flow rate of oxygen. But the parallel flow channel showed significant variation offering better performance at the higher oxygen flow rate. The water formation is more in the exit path of serpentine flow channel, which is resolved by supplying excess oxygen flow rate to drain water formed in the cathode channel.

Many authors published their numerical studies on the single-cell DMFC with serpentine channel but mostly with 1D and 2D models. From the literature, the serpentine flow channel is unmatched by any flow channel in anode for removing gaseous bubbles. And the serpentine is reported not suitable at cathode for water and oxygen management. So the single cell DMFC with different anode and cathode channel is best for rectifying above said issues. The main objective of this paper is to develop a 3Dmathematical model to study the fluid dynamics and electrochemistry of DMFC to predict the performance of a single cell with different flow channels. The influence of various innovative flow channels on the cell performance is investigated and its suitability on anode and cathode side is studied. The existing parallel flow channel is modified by providing triangular distributor at inlet and exit to supply reactant equally to all flow branches. Also, the straight flow path is designed to have the inclination as shown in **Fig. 1** in order to enhance the in-plane flow behavior. This flow channel is named zigzag flow channel.

Similarly, the grid flow channel is modified to have circular ribs as shown in **Fig. 1** to prevent water accumulation in the flow channel and named as pin channel. This paper presents the numerical studies carried out for the following anode-cathode pair of single cell DMFC.

1. Serpentine-serpentine pair (Model I)
2. Zigzag-zigzag pair (Model II)

3. Serpentine-zigzag pair (Model III)
4. Pin type-pin type pair (Model IV)
5. Serpentine-pin type pair (Model V)

The performance enhancement with zigzag and pin channel is compared with conventional serpentine channels to address the merits and demerits of each flow channel at anode and cathode side. With the help of multi-physics software tool, the DMFC performance is predicted by solving all the governing equations such as mass, momentum and species transport combined with electrochemical reactions. The reliability of numerical results is validated against the experimentation on 25 cm^2 DMFC. This model accounts for most of the fluid property variations such as density and viscosity of anode mixture with respect to cell temperature.

Mathematical modelling theory

The single cell DMFC comprises of seven sub-domains which includes anode and cathode flow channels for supplying the reactants, two gas diffusion layers on anode and cathode to distribute the reactants, catalyst layers at anode and cathode for MOR and ORR activity. Along with that, a membrane layer to transport the ions produced during the catalytic action of the anode. All the sub-domains are assembled as shown in **Fig. 2**. The methanol reactant is supplied into the anode flow channel. Methanol reaches the catalyst surface through GDL where it gets oxidized and produces CO^2 as by-product as per the electrochemical reaction given in equation [28].

$$CH_3OH + H_2O \Longrightarrow CO_2 + 6H^+ + 6e^- \quad (1)$$

The electrons are diverted to cathode side through an external circuit and protons are transported to cathode side through the proton exchange membrane (PEM). These electrons combine with protons and oxygen molecules to produce the by-product water as given in equation

$$3/2O_2 + 6H^+ + 6e^- \Longrightarrow 3H_2O \quad (2)$$

The overall cell reaction is expressed as

$$CH_3OH + 3/2O_2 \Longrightarrow 2H_2O + CO_2 \quad (3)$$

The fluid dynamics, species and charge transport mechanism is predicted by solving governing equations on individual domains using the multi-physics commercial software tool. The general governing equations used for modelling DMFC is listed in **Table 1** [23].

In the mass conservation equation, the density of the liquid mixture is calculated for various cell temperatures [28].

$$\rho_l = 1000 - 0.0178(T - 277.15)^{1.7} \quad (4)$$

The momentum equation source term is calculated from the popular Darcy equation, and the mixture viscosity in diffusion term is calculated from the temperature influenced viscosity equation [28].

$$\mu_l = 0.4585 - 5.305 \times 10^{-3}T + 2.31 \times 10^{-5}T^2 - 4.49 \times 10^{-8}T^3 + 3.28 \times 10^{-11}T^4 \quad (5)$$

The molar fractional value of water vapour, oxygen and nitrogen in the air can be calculated from following equations [26].

$$log_{10}P_{sat} = -2.1794 + 0.02953(Y - 273) - 9.1837 \times 10^{-5}(T - 273)^2 + 1.4454 \times 10^{-7}(T - 273)^3 \quad (6)$$

$$Y_{water,in} = \frac{P_{sat}}{P_{total}} \quad (7)$$

$$Y_{O_2,in} = \frac{1-Y_{water,in}}{1+(79/21)} \quad (8)$$

$$Y_{N_2,in} = 1 - Y_{O_2,in} - Y_{water,in} \quad (9)$$

The source term in species conservation equation explains reactant, by-product consumption and generation on both anode and cathode catalyst layers. The mass transport is mainly due to the convection and diffusion mechanism. The effective diffusion of species can be calculated from Ref. [26] the relation

$$D_i^{eff} = \varepsilon^{1.5} D_i \quad (10)$$

The ionic conductivity of membrane in charge conservation equation is given by Ref. [28].

$$\sigma_m = \sigma_m^{ref} exp\left[1268\left(\frac{1}{T_{ref}} - \frac{1}{T}\right)\right] \quad (11)$$

Electrochemical kinetics theory

The ideal cell voltage of single cell DMFC is restricted to 1.21 V and the open circuit voltage achieved is approximated in the range of 0.5-0.7 V. The maximum output power is achieved at the voltage range of 0.3 to 0.15 V. The practical cell performance deviates from the ideal cell voltage due to major issues such as activation, ohmic and concentration overpotential. The actual cell potential can be calculated from the equation [27].

$$E = E_{cell} - \eta_a - \eta_c - IR - IR_{contact} = E_{rev} - \eta_{activation} - \eta_{concentration} - \eta_{ohmic} \quad (12)$$

where, $R = \frac{\delta}{\sigma}$

E_{cell} is the thermodynamic cell potential, which is the difference between anode and cathode potential. This is mainly dependent on reactant pressure and temperature as follows [25].

$$E_{rev} = E_0 = E + \Delta T\left(\frac{\delta E}{\delta T}\right) - \Delta N \frac{RT}{nF} ln\left(\frac{P_2}{P_1}\right) \quad (13)$$

where E_0 is cell equilibrium potential, the second term expresses the cell potential difference for any temperature difference, which can be found using the relation given in **Table 3**. The third term in the equation connects cell potential with reactant supply pressure. The cell potential difference caused by the temperature difference can be calculated from the entropy change during electrochemical reaction as follows [25].

$$\Delta T\left(\frac{\delta E}{\delta T}\right)_P = \Delta T\left(\frac{\delta S}{nF}\right) \quad (14)$$

Activation overpotential on anode side of the DMFC cell is calculated using Butler-Volmer equation as follows [22],

$$I_{anode} = i_a^{ref}\left(\frac{C_a^{MeOH}}{C_a^{MeOH,ref}}\right) exp\left(\frac{\alpha_a F}{RT}\eta_a\right) \quad (15)$$

$$i_a^{ref} = 94.25 exp\left[\frac{35570}{R_u}\left(\frac{1}{353} - \frac{1}{T}\right)\right] \quad (16)$$

where, I^{ref} is reference exchange current density, C^{ref} is reference concentration of reactant, η is overpotential, α is transfer coefficient defined individually for anode and cathode with subscript 'a' and 'c'.

Similarly, Tafel equation is used to find activation overpotential in the cathode side. The cross over current is calculated from the cross over methanol flux.

At cathode side

$$\eta^{c}_{activation} = \left(\frac{RT}{\alpha_c F}\right) ln\left(\frac{i_{cell}+i_{xover}}{i_{oc}}\right) \quad (17)$$

$$i_{oc,ref}\left(\frac{C_g^{O_2}}{C_{g,ref}^{O_2}}\right) \quad (18)$$

$$i_{xover} = 6FN_{MeOH} \quad (19)$$

$$N_{MeOH} = -D^{eff}_{MeOH}\frac{\nabla C_l^{MeOH}}{dx} + \varepsilon\left(\frac{C_l^{MeOH}}{C_l^{Water}+C_l^{MeOH}}\right)\frac{i_{cell}}{F} \quad (20)$$

The concentration overpotential due to the concentration gradient at the catalyst surface is calculated from Nernst equation [22,25,28] where n_a and n_c are number of electron transfer at anode and cathode. The reactant gas concentration at inlet of channel and catalyst surface is taken into account for concentration gradient.

Concentration polarization by Nernst equations [22].

$$\eta^{a}_{concentration} = \left(\frac{RT}{n_a F}\right) ln\left(\frac{C_l^{MeOH}}{C_{l,in}^{MeOH}}\right) \quad (21)$$

$$\eta^{c}_{concentration} = \left(\frac{RT}{n_c F}\right) ln\left(\frac{C_g^{O_2}}{C_{g,in}^{O_2}}\right) \quad (22)$$

The material resistance for electron transport is measured using ohms' law as given by equation (24) where δ and σ denotes thickness and ionic conductivity of the respective cell layers [22],

$$\eta_{ohmic} = i_{cell}\left(\frac{\delta_{acl}}{\sigma_{acl}} + \frac{\delta_m}{\sigma_m} + \frac{\delta_{ccl}}{\sigma_{ccl}}\right) \quad (23)$$

The total efficiency of the cell is calculated accounting all the losses like thermodynamic loss, voltage loss and fuel loss. The total efficiency of cell is formulated as [29].

$$\eta_{total} = \eta_{thermal}\eta_{voltaic}\eta_{farady} = \left(\frac{\Delta g}{\Delta h}\right)\left(\frac{V_{cell}}{V_0}\right)\left(\frac{I}{I+I_{xover}}\right) \quad (24)$$

Numerical procedure

The mathematical model is simplified to solve the governing equations based on the following assumptions.

- ✓ Flow is steady, laminar and isothermal
- ✓ Cathode reactant supply is assumed as ideal gas
- ✓ The effect of CO2 bubble is negligible
- ✓ The membrane is impermeable and fully hydrated

The numerical work is carried out using the commercial software platform COMSOL 5.4 and the CAD design is done in Solidworks 2017. The cell geometry is modelled as per the specifications given in

Table 2. The boundary conditions are specified to solve the governing equations such as flow, species and transport equations. The anode inputs are flow velocity, methanol concentration, mass fraction of water and methanol. The anode and cathode outlet is fixed to zero gauge pressure value. The cathode inputs are air velocity, mass fraction value of Oxygen, Nitrogen and Water. The fluid dynamics equations are coupled with electrokinetic equations to predict the source terms for various input parameters. Flow channels are meshed with hexahedral elements and other layers are meshed with triangular elements. To predict velocity gradient near the solid boundary, the number of boundary layer near the wall is increased to 4. Further, the catalyst layer thickness is divided into 10 times uniformly to predict the large concentration changes on the catalyst surface. The grid independency study is carefully done for fixed voltage of 0.25 V against current density variation. The number of element is varied from 4 to 8 lakhs. Finally, element number of 5, 28,624 is chosen for the model by ensuring the change in current density is negligible above this element number. **Fig. 3 (a)** shows the clear picture of meshed domain. The MUMPS solver is used to solve the differential equations. The current density is calculated for each potential applied on the cathode, and the parametric study is conducted from 0.7 V to 0.1 V for every 0.05 V step interval.

Model validation

The experiment is conducted for 0.5 M methanol concentration, active area of 25 cm2 and cell temperature of 80 ^{o}C. The commercial MEA with anode loading of 4 mgPt-Ru/cm^2 and cathode loading of 0.5 mgPt/cm^2 is purchased from Fuel Cell Store for experimental validation. The experimentation is carried out in Scribner FCT 850e system to predict the performance curve of single cell DMFC. The experimental test setup consists of anode, cathode flow meters, humidifier, heating plug, thermocouple, load bank unit and peristaltic pump. All these measuring devices are calibrated before experimentation as per the manual furnished by Scribner. At first, the cell MEA is activated at constant current density for different magnitudes. The methanol is supplied in anode serpentine flow channel using the Masterflex L/S peristaltic pump, and air is supplied to the cathode flow channel after humidifying it to 100%. The cell voltage is set to open circuit voltage, and current density is noted for every 10 mV per second. From **Fig. 3 (b)**, the numerical results are well aligned with experimentation, and a maximum deviation of 12.2% is observed at a high current density where mass concentration loss is very high. The same modelling procedure is adopted for all other flow channels.

Results and discussion

The flow channel is responsible for the reactant transportation over the catalyst surface. The best flow channel design is identified based on the uniformity in species distribution, minimum pressure drop, effective thermal and water management and effective by-product removal capacity. In DMFC, the challenging task of the flow channel is to remove the gaseous by-product from anode channel and maintain oxygen availability in the cathode as well as handling of water and fuel crossover.

Influence of anode pressure drop

The pressure drop from inlet to exit of the channel influences fuel pumping power and capacity of the channel in removing CO_2 bubble from active surface. Higher magnitude of pressure drop increases pumping power, and lower pressure drop challenges effectiveness of CO_2 bubble removal [18]. So a balanced pressure drop is preferred in flow channel for the stable output power from the DMFC cell. The pressure drop in pin and zigzag channel is observed minimal from **Fig. 4** that is less than 5 Pa. The entry of methanol fuel in these flow channels is branched into many paths and the supplied fuel exits with very short stream path that is not much greater than the length of the cell.

This lessens the pressure drop and makes other minor losses along the flow channel insignificant as can be seen in **Fig. 4**. But in the case of serpentine anode channels, the pressure drop is in the range of 180-600 Pa for different cathode channels taken for study. The anode serpentine channel permits the entire methanol feed to flow from the inlet to exit through a lengthy stream path of around 0.654 m long without any branches. So serpentine flow channel is suffered by larger pressure drop due to lengthy stream path and minor loss along the channel is significant because of more number of channel bends. Higher pressure drop is necessary to remove the gaseous bubbles otherwise it will form slugs which are very difficult to remove [24]. The gas slugs are very hard to remove with low pressure drop, and this reduces MOR activity in anode channel. From the pressure plot, it is evident that pressure difference exists between adjacent flow paths of the serpentine channel. This pressure drop between the channels assists methanol fuel to be transported under the ribs, thereby increasing methanol supply rate over the anode catalyst surface [21]. If the pressure drop between the channels is too high, the transport of fuel under the rib is by convection mechanism rather than diffusion, where the later occur at low pressure drop [38]. Here, the pressure drop in serpentine channel is higher than the zigzag and pin channel. This result in improved convective flux in serpentine (2.5 kg/m^{2}s) compared to zig-zag (1.4 kg/m^{2}s) and pin channel (1.2 kg/m^{2}s). The anode serpentine channel along with cathode zigzag channel (Model III) resulted higher pressure drop. It indicates that more amount of methanol is transported over catalyst surface because zigzag cathode channel assisted in improving ORR activity by supplying uniform oxygen supply and reduced the effect of water formation. The Model III offered higher pressure drop of 600 Pa which improved methanol supply over catalyst surface by shifting mass transport mechanism from diffusion to convection. So, serpentine channel at anode is considered best for fuel and by-product management.

Influence of anode velocity

The serpentine channel attained highest centre line velocity in the channel path compared to any other flow channel considered for study. The velocity profile shows consistent flow from inlet to exit that ensures uniform distribution of methanol over the active surface. This high velocity in the serpentine channel is necessary to remove gaseous by-product formed during the MOR activity. As the fuel passes from inlet to outlet through a lengthy path line, residence time of fuel inside the cell increases [40]. Further, fuel efficiency of the cell is increased by enhancing fuel supply over the catalyst. If methanol is supplied at very high velocity, it reduces residence time of fuel inside the channel, and fuel utilization efficiency reduces. The high velocity of fuel in flow path increases under rib convection, and the low velocity of fuel reduce methanol supply by shifting to diffusion mechanism [15]. The residence time of fuel in other flow channel is less because fuel takes a very short path to exit the channel. So fuel consumption on the catalyst surface is less, and fuel utilization is affected. From **Fig. 5**, pin type channel attained the best centre line velocity between each rib columns, but velocity of fuel between each rib rows is very less and insufficient. From the plot, more stagnant locations are identified in pin channels. Stagnation in the flow channel is more responsible for fuel cross over from anode to cathode. Also, stagnation blocks the gaseous bubbles on GDL surface and cannot be driven out [42]. More bubbles continue to accumulate and reduce the fuel supply for MOR activity. This phenomenon reduces fuel utilization, thus reducing fuel cell performance. The zigzag channel suffers from same problems and fuel supply lags in uniformity because the triangular distributor failed to supply constant feed of methanol to all flow paths. As the pressure difference between adjacent channels is negligible, the advantage of under rib fuel supply is affected [15]. This reduces uniformity in fuel supply over the catalyst surface. The flow channel exit converges to minimal size resulting into the high possibility of eddy formation. If the cell is operated at high methanol feed rate, there is a possibility of turbulence at channel exit. Whereas,

serpentine channel flow is completely streamlined from inlet to exit and the flow remains laminar. Even though the flow channel is symmetrical in zigzag and pin channel, the sudden expansion of flow through small opening breaks the symmetry during bifurcation. And this phenomenon is the common occurrence in fuel cell entry regions as reported in Jithin et al. [45]. This asymmetry bifurcation is visible on top right side and left side of zigzag and pin channel velocity contour. From **Fig. 5**, the model containing serpentine channel at anode exhibited uniform methanol supply from inlet to exit without any stagnation point. So anode serpentine channel is considered best for uniform supply of methanol.

Influence of cathode pressure drop

In the cathode side, ORR activity is initiated by supplying air with saturated condition (RH 100%) into the cathode channel. Pin channel achieved a very low pressure drop of less than 50 Pa. Pressure gradient is observed very less except for the exit channel. As the gas enters into flow channel, it expands due to the diffuser used for distributing the air. The expanded gas further expands into the channel path and continues to converge towards exit. As air is consumed in the channel path, the air pressure is maintained constant towards the exit. Since water formation is very much reduced, the drag loss by water droplets is expected to be minimal. From **Fig. 6**, serpentine cathode channel achieved a pressure drop threefold higher than pin channel. The high-pressure drop is attributed due to lengthy streamlines of flow and significant minor losses along the flow path [22]. Water droplets produced in cathode channels increases the pressure drop along with other minor losses like channel bend, inlet and exit loss. The water collected from each channel path accumulates to maximum at the exit. More water drops at the exit increase drag loss as the flow continues. But a high-pressure drop is required for serpentine flow channel to sweep away the water formed in the cathode channels as well as water droplets under the ribs. The pressure difference between the paths assists in removing these water droplets diffused under the ribs. The serpentine channel is to be supplied with excess air to compensate oxygen requirement as well as to remove water droplets from the flow channels. The local pressure drop inside the channel increases complexity of water handling by allowing water to condense and evaporate to maintain saturation level during the course of flow. Zigzag flow path distributes incoming flow rate into different paths that reduce the pressure drop. This result in uniform pressure in flow channel and maximum velocity inside channel path is reduced, owing to an increase in reactant residence time. Further, the reactant utility for ORR activity is improved [41]. The water droplets formed throughout the channel is uniform and lesser water accumulation compared to serpentine channel. Thus increases ORR activity, which eventually increases the cell output power. It is concluded that the pin and zigzag flow channel is best on cathode side since the pressure drop is very low (less than 50 pa) and pressure is same throughout the flow channel.

Influence of cathode velocity

Serpentine flow channel in cathode attained the highest line velocity along the flow path compared to all other flow channels taken for study. The velocity of the flow in serpentine channel is uniform except some of the channels in the middle. The main reason is that oxygen is consumed higher at the inlet, which increases the water content of the air [43].Water reaches the saturation level, and then it starts to condense. This reduces velocity in the midway of channel. The flow gains momentum and causes a pressure drop further. In Some local points along the channel path, water condensation and evaporation begins that raises the concern of flooding and starvation [39]. Methanol solution transported under the rib of anode channel cannot access sufficient oxygen under the rib of cathode channel. Therefore, a concentration gradient is created on the catalyst surface which degrades cell performance. From **Fig. 7**, Pin channel has uniform velocity along the

flow line yet showed more stagnation points around the circular ribs [22]. It reduces oxygen supply over the catalyst surface and reduces utilization of active surface. The zigzag flow path has an uneven velocity in the channel paths. Some of the channels are subjected to insufficient flow rate. The inlet and exit distributor of flow channel is exposed to high velocity of flow, but the channel path has less velocity, which forces reactant over the catalyst surface. The serpentine flow channel at cathode exhibits uniform flow supply without any stagnation point in the flow path. But the zigzag flow path results uneven velocity profile among different flow paths. So serpentine is considered best for cathode fuel supply.

Influence of oxygen concentration

The oxygen concentration on cathode decides the ORR activity, which can be ensured by better oxygen availability. The serpentine channel has reduced oxygen level from inlet to exit, thus creating an oxygen concentration gradient [43]. The last few channels undergo oxygen starvation which increases the concentration loss at the exit as observed in **Fig. 8**. In other words, the excess water formed at the end of channel diminishes reduction reaction by blocking the active surface [41]. So reduction reaction (ORR) is not uniform, thus the cell cathode performance is reduced. The other flow fields exhibited better and uniformed oxygen concentration that assists in improved cathode reaction than serpentine channel. Irrespective of any anode flow channel, pin and zigzag cathode flow channels supplied constant oxygen feed throughout the cathode surface. The oxygen concentration in pin channel is better over the catalyst layer compared to zigzag flow channel. The main reason is that the flow under zigzag channel is greatly affected by reduced pressure drop between the paths, which affects oxygen supply under the ribs. But pin channel is not suffered by the under-rib convection loss because of its short-sized pins [22]. More uniformity in the flow channels is obtainable, possibly through generation of backpressure at the exit of the flow channels. Many studies revealed that backpressure increased the reduction reaction and increased cell performance. But backpressure increase the complexity of water removal and accumulation of water leads to a reduction in cell performance. So, balanced back pressure has to be predicted to operate the cell for high performance. The fuel uniformity is assessed by the concentration gradient. The concentration gradient of serpentine channel (2.1 m^{-1}) is higher than the zigzag (0.0016 m^{-1}) and pin channel (0.04 m^{-1}). The pin and zigzag channels are identified as suitable cathode channel by effectively maintaining uniform oxygen supply whereas the serpentine flow channel is inefficient in cathode side.

Influence of water formation

Water formation heavily retards the ORR activity on the cathode side. The serpentine flow channel has excess oxygen availability at inlet and reduced availability at exit. This directly expresses that the water formation at inlet is high. The exit channel gets affected by water accumulation as shown in **Fig. 9**, thus blocks the utility of oxygen level at exit channel [39]. Higher water formation at the mid-channel, higher the possibility of flooding at exit and higher water evaporation reduces cell temperature. Subsequently, the electrochemical reaction rate reduces significantly [18]. In case of pin and zigzag channels, water formation is less in channels, and water distribution is more uniform from inlet to exit. In zigzag flow, channel does not have a significant pressure drop between the adjacent paths. The water diffusion under the rib is limited, and oxygen supply is not affected. The flow velocity distributes oxygen and balances water formation. This enhances the cathode cell reaction. The possibility of unexpected condensation and evaporation is reduced by having uniform pressure over the entire flow channel using backpressure method [44]. The serpentine channel path at the exit has more water concentration. The zigzag and pin channel exhibited best water removal capacity and worthy to be cathode flow channel.

Performance analysis of DMFC cell

The current density and power density for different flow channel configurations are shown in **Fig. 10**. The serpentine flow channel (Model I) on anode and cathode yielded 34 mW/cm^2 of power density which is more than the pin (Model Ⅳ) and zigzag (Model II) flow channels. The serpentine channel in anode distributes methanol more uniformly over the catalyst surface and assists flow under the rib, which enhanced the fuel consumption. This led to improved MOR activity on the anode side. On the other hand, serpentine channel on the cathode side failed to remove water from flow channel thus causing reduced reduction rate. The oxygen level also dropped from inlet to exit resulting in oxygen reduction and starvation at the exit. Also, the local pressure drop in cathode alters the moisture level of air which causes water in flow channel to evaporate and condensate. The water flooding and water starvation at the local point leads to reduced reaction rate, resulting in reduced cell performance. Pin channel has a uniform velocity profile between the columns and nonuniformity in velocity between the rows in both anode and cathode. The local stagnation inside the channel increases methanol crossover rate thus increases the parasitic loss. The maximum velocity attained in the pin channel is low because of distributed flow. So, the oxidation reaction of methanol is poor. But the pin channel placed in cathode side exhibited better performance by maintaining the oxygen availability. The pin channel also assisted in handling water droplets from cathode side and maintained constant water level leading to a better cathode reaction. Hence, the pin channel is preferred as cathode channel and serpentine channel as anode, which showed a 10.2% improved cell performance as indicated in **Table 4**. The problem of cathode flooding and methanol crossover can be surpassed by keeping the pin channel in cathode side. Similarly, zigzag flow field expressed non-uniform methanol distribution in the anode channel with reduced pressure drop. The lower pressure drop is insufficient to remove the gaseous slugs formed in the channel path when operating the cell at a low methanol flow rate. But the zigzag flow field is advantageous in cathode side by effectively maintaining water and oxygen level in the flow path. With the serpentine channel as anode, and zigzag flow channel as cathode, the merits of both flow channels were utilized. It revealed improved power density of 40.13 mW/cm^2. It is 17.8% higher than the cell having serpentine channels on both sides. From the performance, usage of two different flow channels (serpentine-zigzag) at anode and cathode is promising the performance improvement by uniform supply of reactant and effective water management.

Conclusion

A 3D mathematical model was developed to analyze the performance of innovative flow fields like zigzag and pin channels. The model was validated against the in-house experimentation results. From anode perspective, the serpentine is more competent than any other flow channels considered. The zigzag flow channel had non-uniform methanol flow, and pin channel had more stagnation points. The serpentine anode channel had uniform flow distribution, and under rib flow convection between flow paths, which increased reactant supply over the catalyst layer. From the pressure contours, it is evident that the pressure drop in the serpentine is high, which is required to drive off the CO_2 bubbles from the flow paths. But the water removal and air supply uniformity on cathode is better in zigzag and pin channels. The serpentine channel had increased water content at the exit of flow path leading to concentration loss. So a single-cell DMFC made with serpentine anode channel and zigzag cathode (Model III) channel revealed an improved power density of 40.13 mW/cm2. This results in 17.8% better than the cell with only serpentine flow channels because of better reactant supply and increased ORR activity. The cathode pin channel and anode serpentine channel combination (Model Ⅴ) achieved 10.2% improved cell performance by effective water management and uniform reactant supply. Although, the numerical results promised enhanced

power density, the overall cell resistance, contact resistance between MEA and flow channel, activation overpotential effect and cell impedance should be studied carefully. The post MEA condition after experimentation and durability study is to be ensured for stacking. Along with that, the practical difficulties such as torque required for cell assembly, manufacturing difficulties of flow channel, sudden expansion of fuel inside the channel is to be studied experimentally for further development.

Declaration of competing interest

The authors declare that they have no known competing financial interests or personal relationships that could have appeared to influence the work reported in this paper.

Acknowledgement

The experimental work is financially supported by DSTUKIERI project (DST/INT/UK/P121/2016) partnership with Loughborough University, U.K and PSG College of Technology, India.

Reference

[1] Achmad F, Kamarudin SK, Daud WR, Majlan EH. Passive direct methanol fuel cells for portable electronic devices. Appl Energy 2011;88:1681-9.

[2] Ismail A, Kamarudin SK, Daud WR, Masdar S, Hasran UA. Development of 2D multiphase non-isothermal mass transfer model for DMFC system. Energy 2018;152:263-76.

[3] Ong BC, Kamarudin SK, Basri S. Direct liquid fuel cells: a review. Int J Hydrogen Energy 2017;42:10142-57.

[4] Alias MS, Kamarudin SK, Zainoodin AM, Masdar MS. Active direct methanol fuel cell: an overview. Int J Hydrogen Energy 2020;45(38):19620-41.

[5] Kamaruddin MZ, Kamarudin SK, Daud WR, Masdar MS. An overview of fuel management in direct methanol fuel cells. Renew Sustain Energy Rev 2013;24:557-65.

[6] Calabriso A, Borello D, Romano GP, Cedola L, Del Zotto L, Santori SG. Bubbly flow mapping in the anode channel of a direct methanol fuel cell via PIV investigation. Appl Energy 2017;185:1245-55.

[7] Su X, Yuan W, Lu B, Zheng T, Ke Y, Zhuang Z, Zhao Y, Tang Y, Zhang S. CO2 bubble behaviors and two-phase flow characteristics in single-serpentine sinusoidal corrugated channels of direct methanol fuel cell. J Power Sources 2020;450:227621.

[8] Goor M, Menkin S, Peled E. High power direct methanol fuel cell for mobility and portable applications. Int J Hydrogen Energy 2019;44(5):3138-43.

[9] Xu Q, Zhao TS, Yang WW, Chen R. A flow field enabling operating direct methanol fuel cells with highly concentrated methanol. Int J Hydrogen Energy 2011;36(1):830e8-

[10] Hsieh SS, Wu HC, Her BS. A novel design for a flow field configuration, of a direct methanol fuel cell. J Power Sources 2010;195(10):3224-30.

[11] Ramesh V, Krishnamurthy B. Modeling the transient temperature distribution in a direct methanol fuel cell. J Electroanal Chem 2018;809:1-7.

[12] Park YC, Chippar P, Kim SK, Lim S, Jung DH, Ju H, Peck DH. Effects of serpentine flow-field designs with different channel and rib widths on the performance of a direct methanol fuel cell. J Power Sources 2012;205:32-47.

[13] Kianimanesh A, Yu B, Yang Q, Freiheit T, Xue D, Park SS. Investigation of bipolar plate geometry on direct methanol fuel cell performance. Int J Hydrogen Energy 2012;37(23):18403-11.

[14] Ouellette D, Ozden A, Ercelik M, Colpan CO, Ganjehsarabi H, Li X, Hamdullahpur F. Assessment of different bio-inspired flow fields for direct methanol fuel cells through 3D modeling and experimental studies. Int J Hydrogen Energy 2018;43(2):1152-70.

[15] Yang Y, Liang YC. Modelling and analysis of a direct methanol fuel cell with under-rib mass transport and two-phase flow at the anode. J Power Sources 2009;194:712-29.

[16] Turkmen AC, Celik C, Esen H. The statistical relationship between flow channel geometry and pressure drop in a direct methanol fuel cell with parallel channels. Int J Hydrogen Energy 2019;44(34):18939-50.

[17] Yuan W, Wang A, Ye G, Pan B, Tang K, Chen H. Dynamic relationship between the CO2 gas bubble behaviour and the pressure drop characteristics in the anode flow field of an active liquid-feed direct methanol fuel cell. Appl Energy 2017;188:431-43.

[18] Oliveira VB, Rangel CM, Pinto AM. Effect of anode and cathode flow field design on the performance of a direct methanol fuel cell. Chem Eng J 2010;157:174-80.

[19] Park SM, Kim SK, Lim S, Jung DH, Peck DH, Hong WH. Experimental investigation of current distribution in a direct methanol fuel cell with serpentine flow-fields under various operating conditions. J Power Sources 2009;194(2):818-23.

[20] Hu XQ, Yang QW, Xiao G, Chen XT, Qiu X. Power generation enhancement in direct methanol fuel cells using nonuniform cross-sectional serpentine channels. Energy Convers Manag 2019;188:438-46.

[21] El-Zoheiry RM, Ookawara S, Ahmed M. Efficient fuel utilization by enhancing the under-rib mass transport using new serpentine flow field designs of direct methanol fuel cells. Energy Convers Manag 2017;144:88-103.

[22] Ouellette D, Gencalp U, Colpan CO. Effect of cathode flow field configuration on the performance of flowing electrolyte direct methanol fuel cell. Int J Hydrogen Energy 2017;42:2680-90.

[23] Jung S. Direct methanol fuel cell with interdigitated anode for operating under ultra-low fuel stoichiometry condition. Int J Hydrogen Energy 2015;40:1923-34.

[24] Yuan W, Wang A, Yan Z, Tan Z, Tang Y, Xia H. Visualization of two-phase flow and temperature characteristics of an active liquid-feed direct methanol fuel cell with diverse flow fields. Appl Energy 2016;179:85-98.

[25] Yan TZ, Jen TC. Two-phase flow modelling of liquid-feed direct methanol fuel cell. Int J Heat Mass Tran 2008;51:1192-204.

[26] Roshandel R, Arbabi F, Moghaddam GK. Simulation of an innovative flow-field design based on a bio-inspired pattern for PEM fuel cells. Renew Energy 2012;41:86-95.

[27] Falc~ao DS, Oliveira VB, Rangel CM, Pinto AM. Experimental and modeling studies of a micro direct methanol fuel cell. Renew Energy 2015;74:464-70.

[28] Matar S, Ge J, Liu H. Modelling the cathode catalyst layer of a direct methanol fuel cell. J Power Sources 2013;243:195-202.

[29] Lee J, Lee S, Han D, Gwak G, Ju H. Numerical modeling and simulations of active direct methanol fuel cell (DMFC) systems under various ambient temperatures and operating conditions. Int J Hydrogen Energy 2017;42:1736-50.

[30] Heidary H, Abbassi A, Kermani MJ. Enhanced heat transfer with corrugated flow channel in anode side of direct methanol fuel cells. Energy Convers Manag 2013;75:748-60.

[31] Sun J, Zhang G, Guo T, Jiao K, Huang X. A three-dimensional multi-phase numerical model of DMFC utilizing Eulerian-Eulerian model. Appl Therm Eng 2018;132:140-53.

[32] Mallick RK, Thombre SB, Kothekar KP. An integral mathematical model of liquid feed passive DMFCs with non-isothermal effects and charge conservation phenomenon. J Cleaner Production 2018;182:654-71.

[33] Garcı´a-Salaberri PA, Vera M. On the effect of operating conditions in liquid-feed direct methanol fuel cells: a multi-physics modeling approach. Energy 2016;113:1265-87.

[34] Yang WW, Zhao TS, Xu C. Three-dimensional two-phase mass transport model for direct methanol fuel cells. Electrochim Acta 2007;53:853-62.

[35] Gwak G, Kim D, Lee S, Ju H. Studies of the methanol crossover and cell performance behaviors of high temperature-direct methanol fuel cells (HT-DMFCs). Int J Hydrogen Energy 2018;43:13999-4011.

[36] Fang S, Zhang Y, Ma Z, Sang S, Liu X. Systemic modeling and analysis of DMFC stack for behavior prediction in system level application. Energy 2016;112:1015-23.

[37] Yuan Z, Yang J, Li X, Wang S. The micro-scale analysis of the micro direct methanol fuel cell. Energy 2016;100:10-7.

[38] Cheng CH, Fei K, Hong CW. Computer simulation of hydrogen proton exchange membrane and direct methanol fuel cells. Comput Chem Eng 2007;31(4):247-57.

[39] Lu Y, Reddy RG. Performance of micro-PEM fuel cells with different flow fields. J Power Sources 2010;195(2):503-8.

[40] Nam JH, Lee KJ, Sohn S, Kim CJ. Multi-pass serpentine flowfields to enhance under-rib convection in polymer electrolyte membrane fuel cells: design and geometrical characterization. J Power Sources 2009;188(1):14-23.

[41] Saco SA, Raj RT, Karthikeyan P. A study on scaled up proton exchange membrane fuel cell with various flow channels for optimizing power output by effective water management using numerical technique. Energy 2016;113:558-73.

[42] Wang SJ, Huo WW, Zou ZQ, Qiao YJ, Yang H. Computational simulation and experimental evaluation on anodic flow field structures of micro direct methanol fuel cells. Appl Therm Eng 2011;31(14e15):2877-84.

[43] Li W, Zhang Q, Wang C, Yan X, Shen S, Xia G, Zhu F, Zhang J. Experimental and numerical analysis of a three-dimensional flow field for PEMFCs. Appl Energy 2017;195:278-88.

[44] Karthikeyan P, Velmurugan P, George AJ, Kumar RR, Vasanth RJ. Experimental investigation on scaling and stacking up of proton exchange membrane fuel cells. Int J Hydrogen Energy 2014;39(21):11186-95.

[45] Jithin M, Mishra A, De A, Das MK. Numerical study of bifurcating flow through sudden expansions: effect of divergence and geometric asymmetry. Int J Adv Eng Sci Appl Math 2016;8(4):259-73.

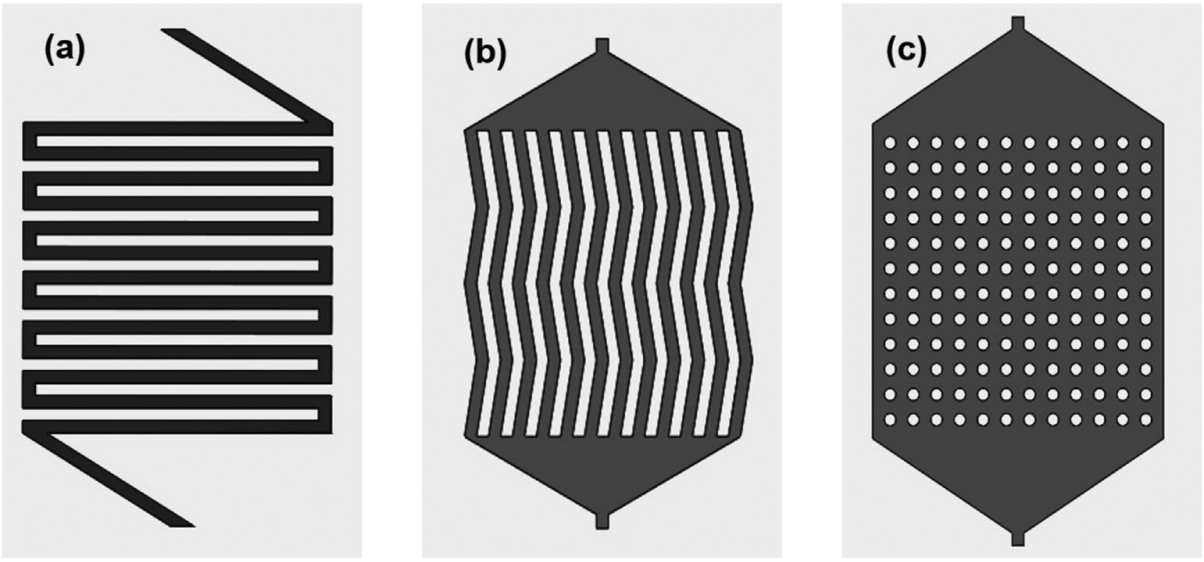

Figure 1 Existing and modified geometry of flow channels (a) serpentine channel (b) Zigzag channel (c) Pin channel.

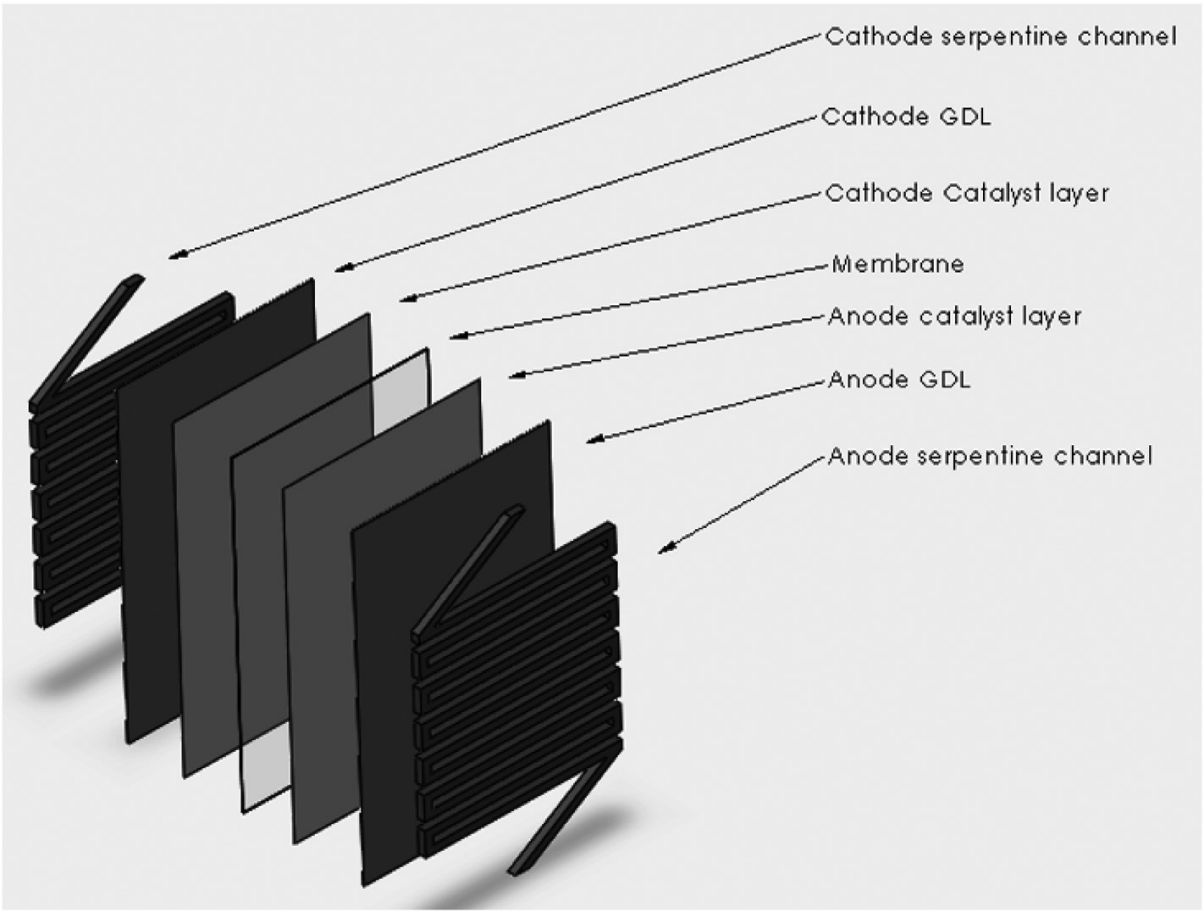

Figure 2 Expanded view of three dimensional DMFC model.

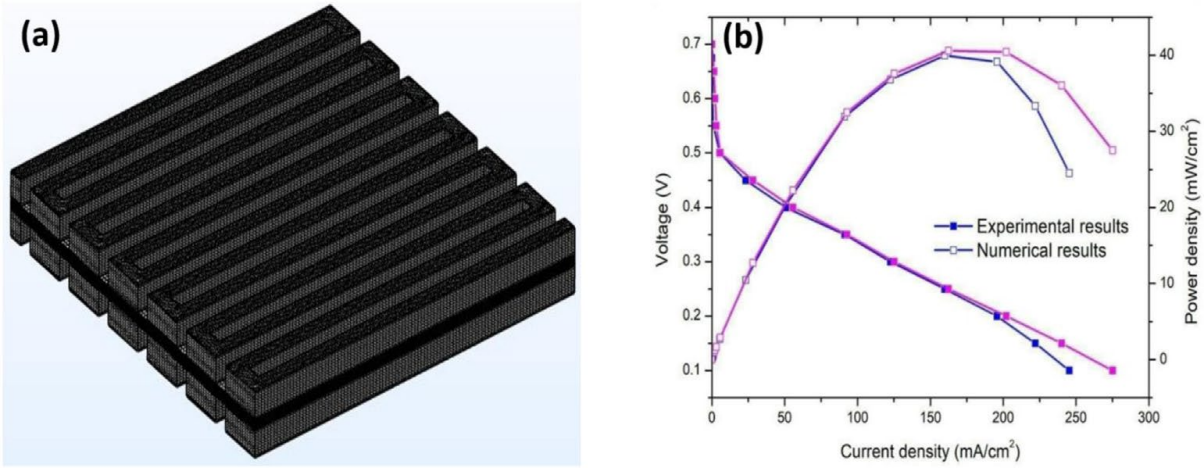

Figure 3 (a) Numerical model (b) Experimental validation of numerical result.

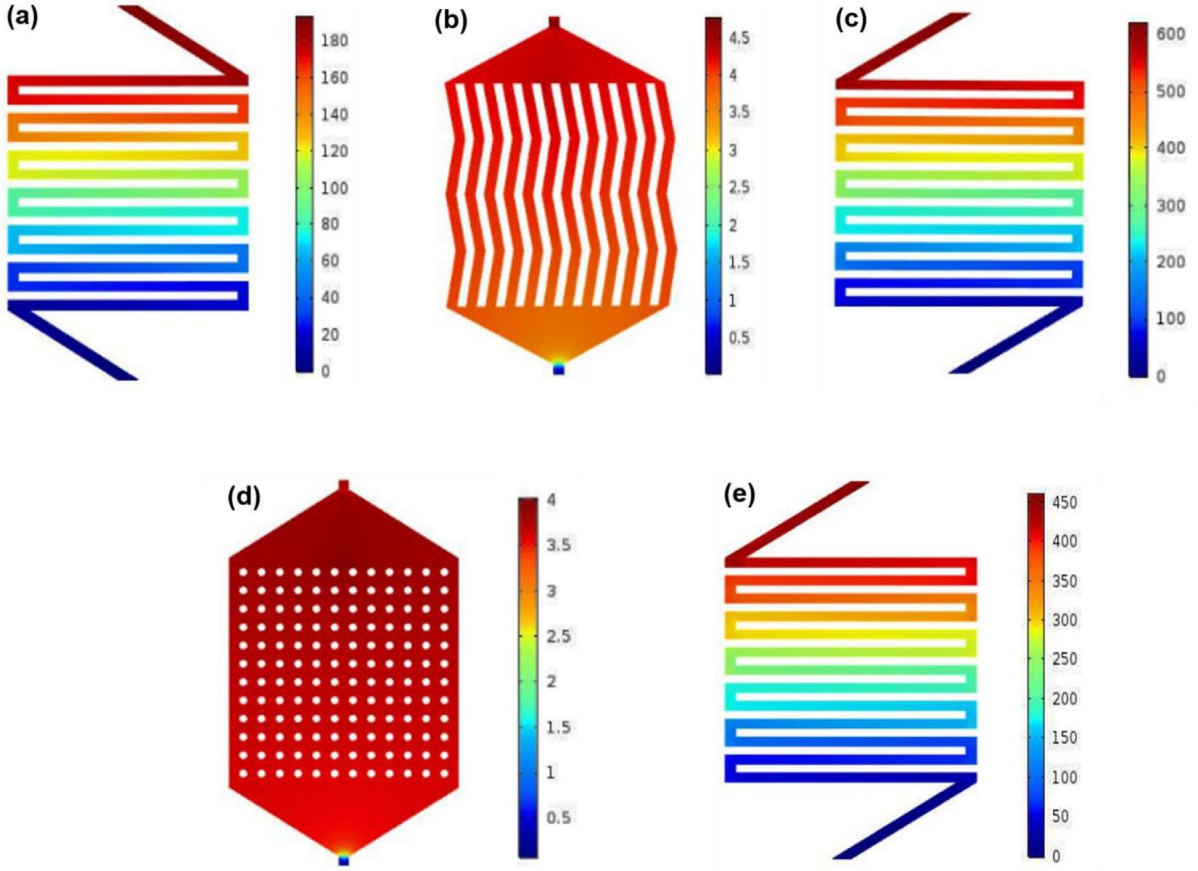

Figure 4 Simulated anode pressure (in Pascal) contours of various DMFC flow channel pairs (a) Model I (b) Model II (c) Model III (d) Model IV (e) Model V.

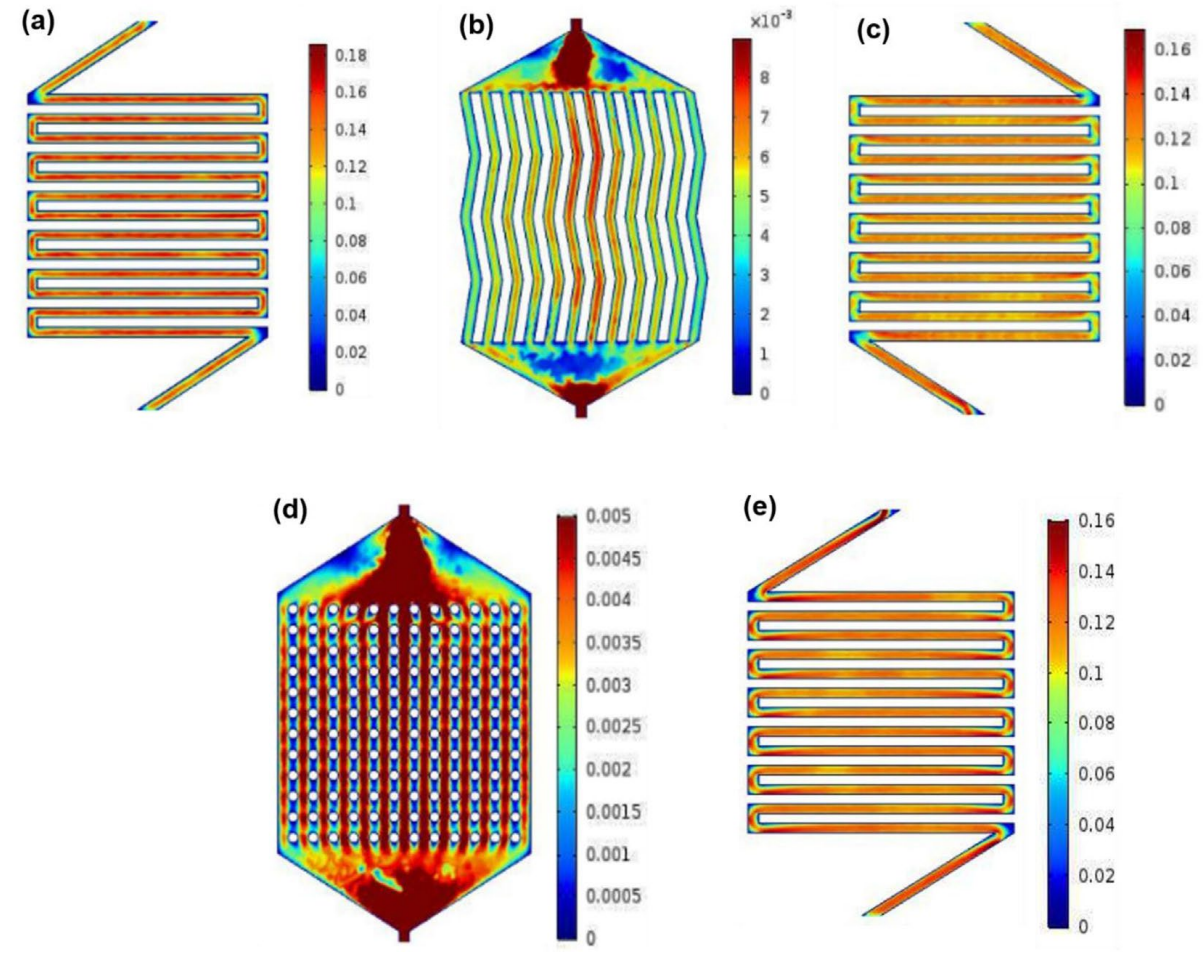

Figure 5 Simulated anode velocity (msi1) contours of various DMFC flow channel pairs (a) Model I (b) Model II (c) Model III (d) Model IV (e) Model V.

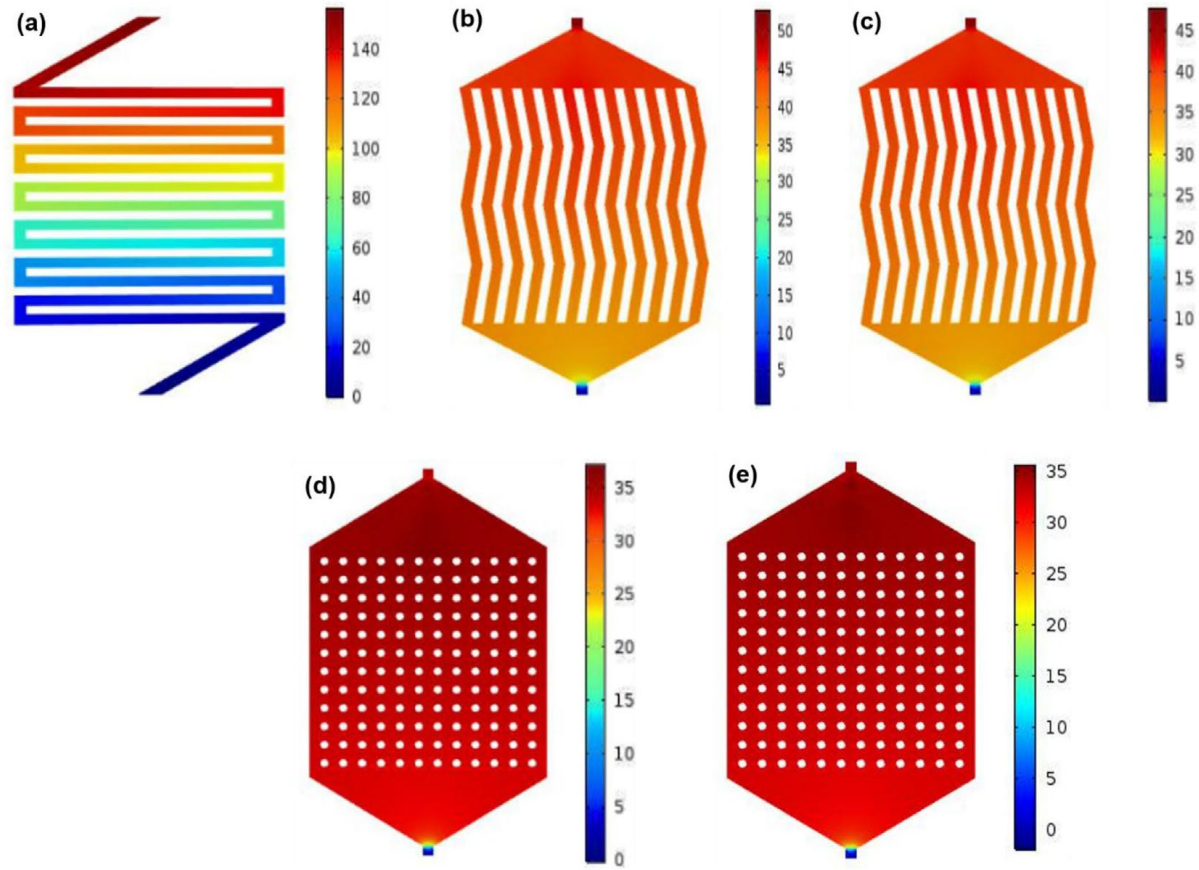

Figure 6 Simulated cathode pressure (in Pascal) contours of various DMFC flow channel pairs (a) Model I (b) Model II (c) Model III (d) Model IV (e) Model V.

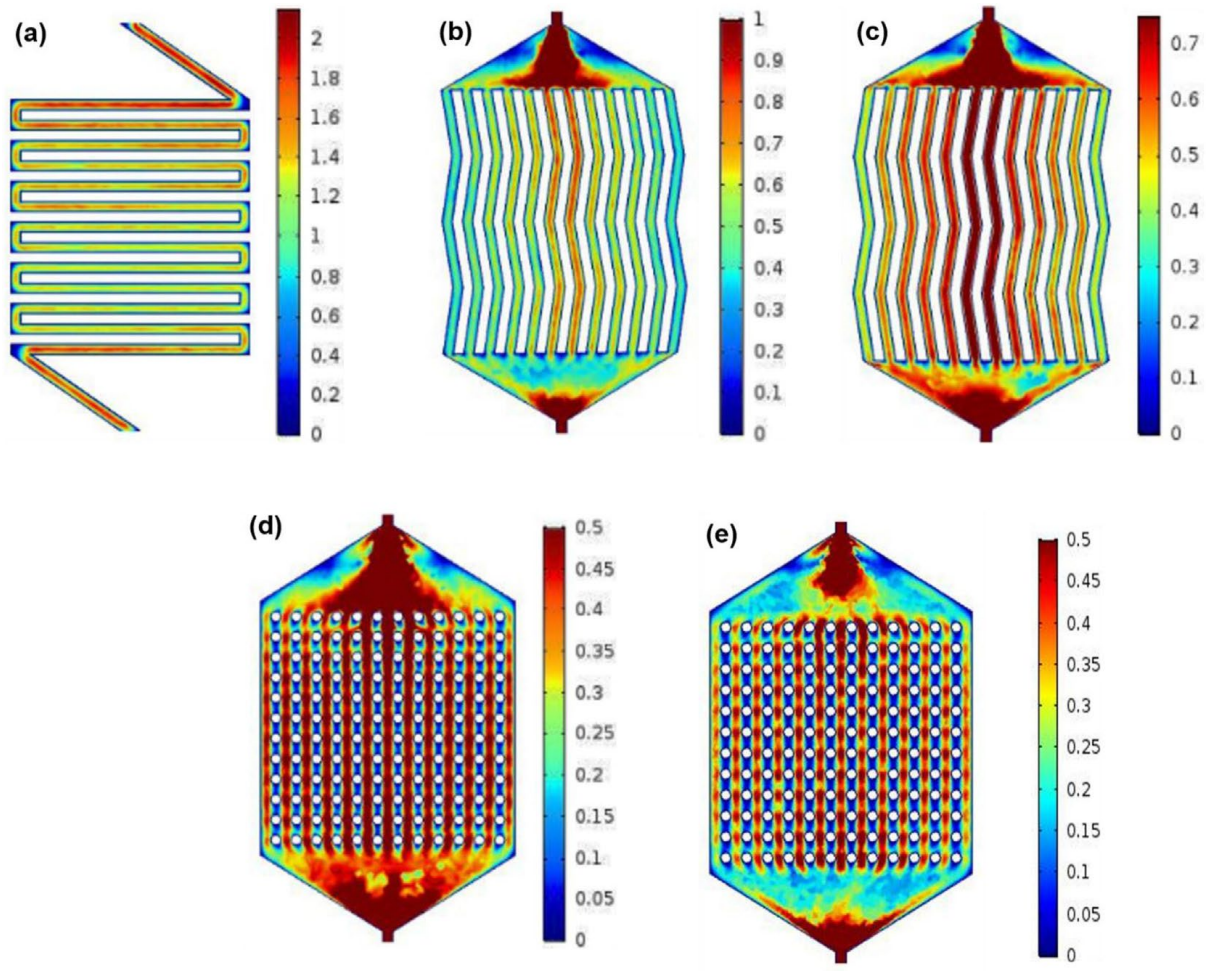

Figure 7 Simulated cathode velocity (ms¡1) contours of various DMFC flow channel pairs (a) Model I (b) Model II (c) Model III (d) Model IV (e) Model V.

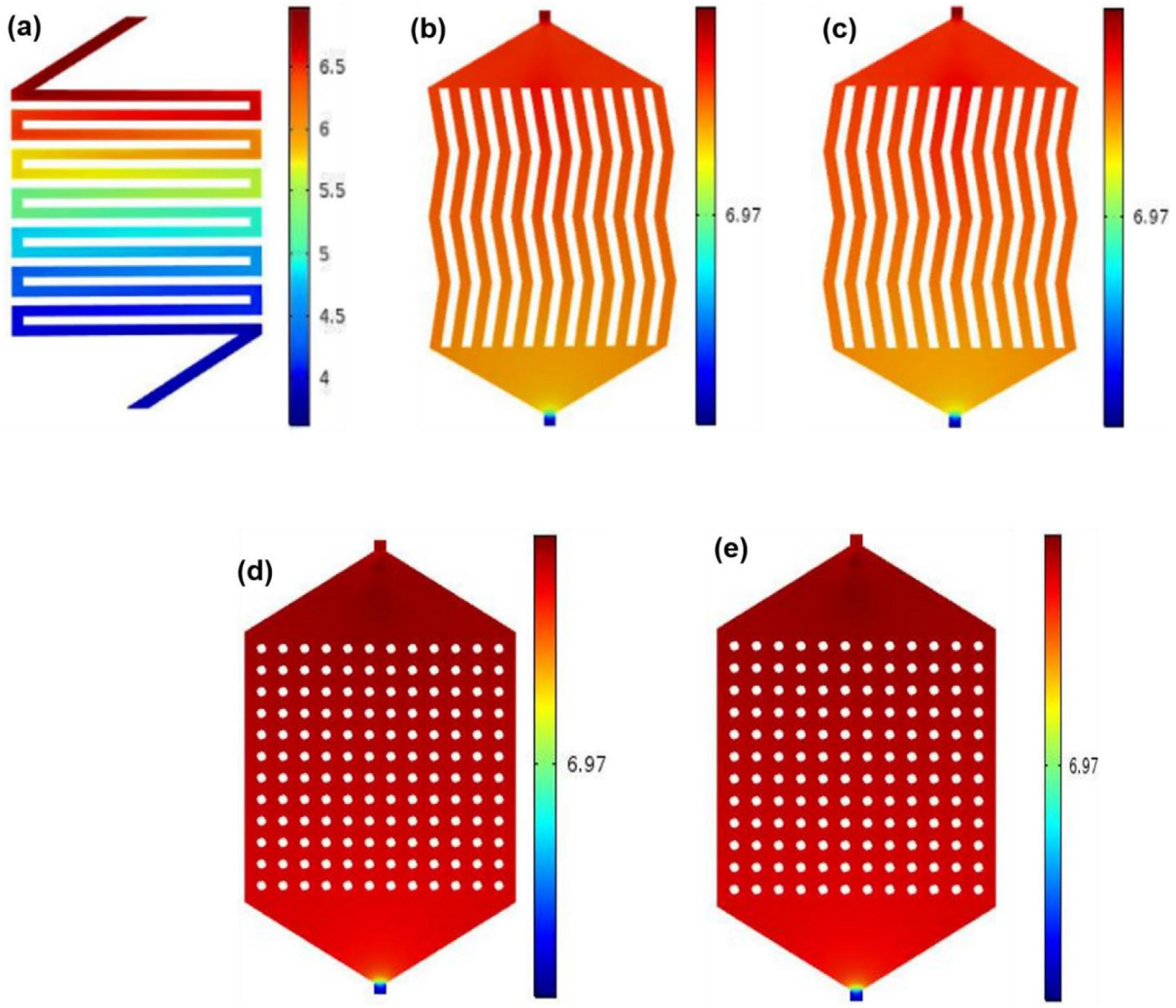

Figure 8 Simulated cathode Oxygen concentration (mol.mj3) contours of various DMFC flow channel pairs (a) Model I (b) Model II (c) Model III t(d) Model IV (e) Model V.

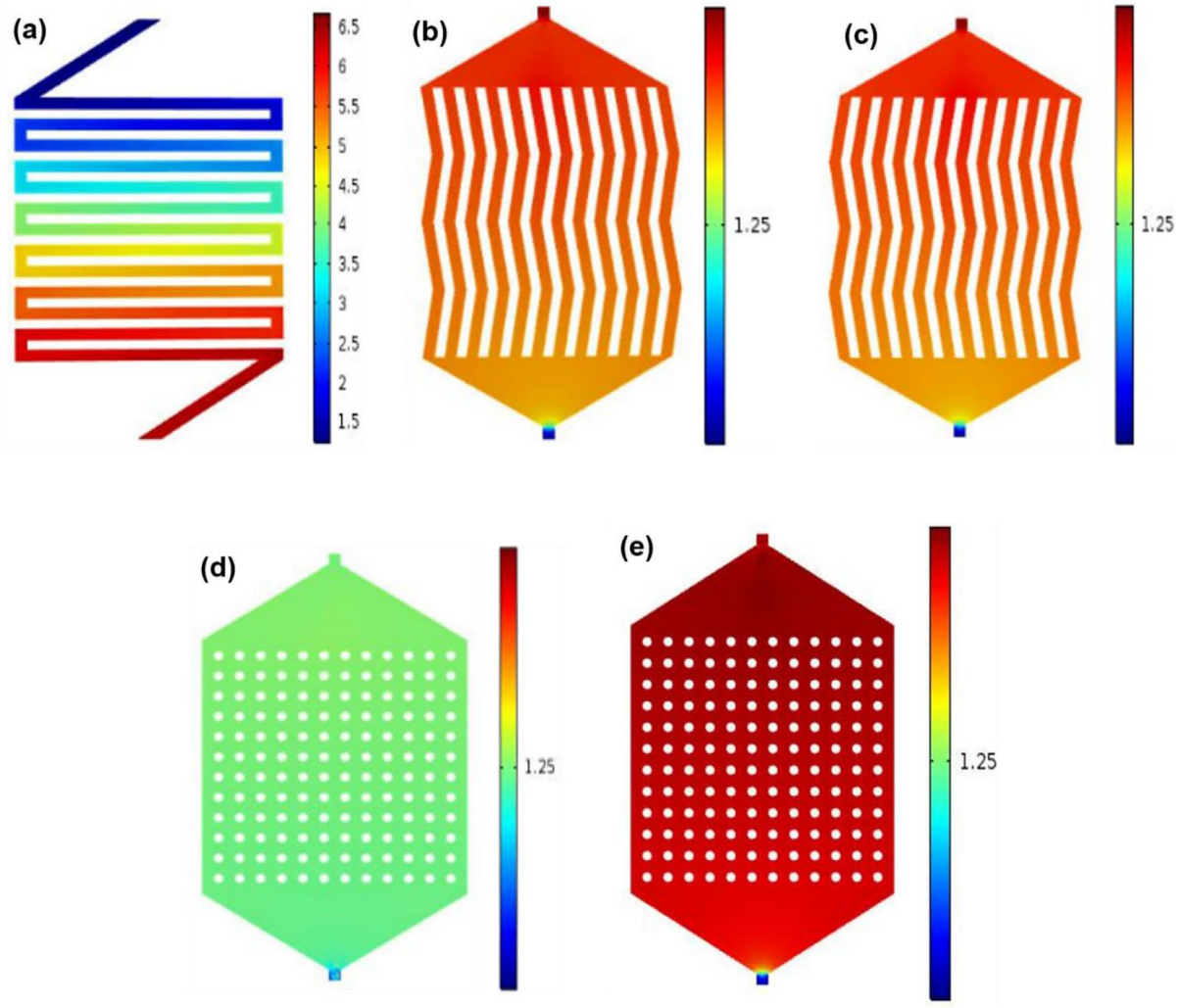

Figure 9 Simulated cathodeWater concentration contours (mol.mi3) of various DMFC flow channel pairs (a) Model I (b) Model II (c) Model III (d) Model IV (e) Model V.

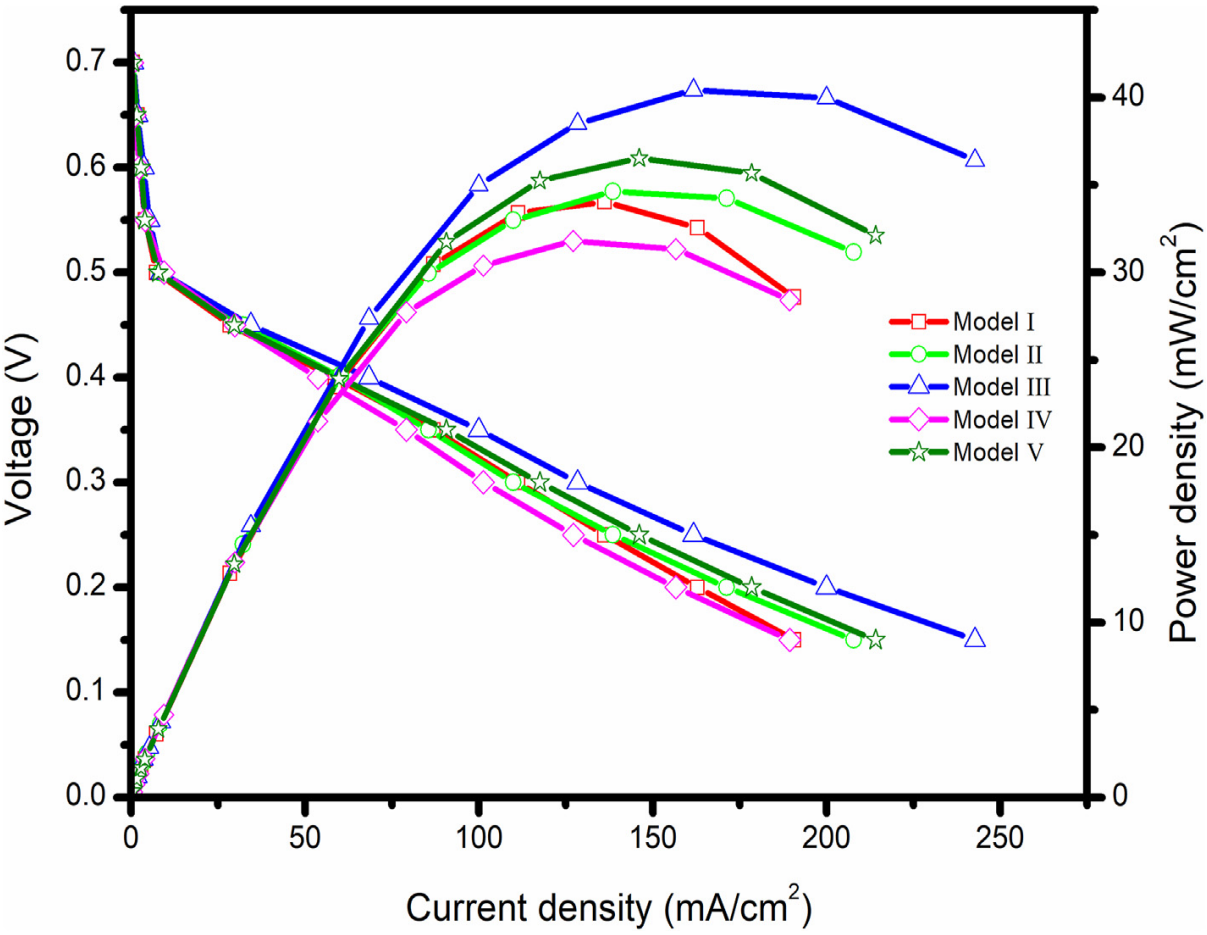

Figure 10 Polarization curve comparison of various DMFC models.

Table 1 - Governing equations for DMFC model.	
Conservation terms	Governing equations
Mass	$\nabla(\rho u) = S^m$
Momentum	$\nabla(\rho u u) = -\nabla P + \nabla\left(\mu^{eff}\nabla \mathrm{u}\right) + S^u$
Energy	$(\rho C_P)(u \cdot \nabla \mathrm{T}) = \nabla\left(k^{eff}\nabla \mathrm{T}\right) + S^T$
Species	$\nabla(\gamma \rho u Y_i) = \nabla\left(\rho D^{eff}\nabla Y_i\right) + S^s$
Proton	$\nabla\left(\sigma_e^{eff}\nabla\varphi_e\right) = S^P$
Electron	$\nabla\left(\sigma_s^{eff}\nabla\varphi_s\right) = S^e$
Governing equations to be solved for DMFC model	

Table 2 - Dimensions of the computational model.		
Geometry parameter	Value	Reference
Size of the cell (A)	5 cm × 5 cm (25 cm^2)	Assumed
Land to channel ratio (L:C)	2:2	Assumed
Channel size (Rectangular type)	2 mm × 2 mm	Assumed
Thickness of anode and cathode catalyst layer (δ_{axl} & δ_{ccl})	60 μm	[37]
Thickness of anode and cathode gas diffusion layer ($\delta_{a,gdl}$ & $\delta_{c,gdl}$)	300 μm	[32]
Thickness of membrane (Nafion 117) (δ_{mem})	180 μm	[31]
Porosity of GDL, CL ($\varepsilon_{gdl}, \varepsilon_{CL}$)	0.7, 0.3	[30,33]
Permeability of GDL, CL,	1.18 x 10^{-11} m^2	[12,28]
Membrane	2.36 x 10^{-12} m^2 5 x 10^{-19} m^2	
Volume fraction of Nafion solution in the catalyst layer	0.25	[31]
Geometry dimension and properties of computational domain.		

Table 3 e Summary of details required for simulation of DMFC model.

Parameter	Value	Reference
Density of methanol ($\rho_{methanol}$)	785 [kg/m^3]	[30]
Viscosity of methanol ($\mu_{methanol}$)	0.0005495 [kg/m.s]	[30]
Density of water (ρ_{water})	998.2 [kg/m^3]	[30]
Viscosity of water (μ_{water})	0.001003 [kg/m.s]	[30]
Viscosity of air (μ_{air})	2.03 x 10^{-5} [kg/m.s]	[33]
Density of membrane (ρ_{mem})	1980 [kg/m^3]	[31]
Anode potential (E_{anode})	0.03 V	[32]
Cathode potential ($E_{cathode}$)	1.24 V	[32]
$\delta E/\delta T$	-1.4 x 10^{-4} [V/K]	[32]
Anode cell potential (E_{anode})	(408.22 x T - 131350)/(6 x F) V	[37]
Cathode cell potential ($E_{cathode}$)	(285830 x 3 - 489.52 x T)/(6 x F) V	[37]
Methanol flow rate ($Q_{methanol}$)	10 ml/min	Assumed
Air flow rate (Q_{air})	600 ml/min	Assumed
Molar concentration of oxygen at the inlet of cathode channel	7.2467 [mol/m^3]	[22]
Reference Molar concentration of methanol ($C_{methanol}$)	100 [mol/m^3]	[31]
Reference Molar concentration of water (C_{water})	56,000 [mol/m^3]	[31]
Reference Oxygen Molar concentration (C_{oxygen})	0.21 x P_{atm}/(R x T) [mol/m^3]	[36]
Anode transfer coefficient (α_a)	0.5	[34]
Cathode transfer coefficient (α_c)	1	[34]
Anode reaction order (γ_a)	0.5	[31]
cathode reaction order (γ_c)	1	[31]
Faraday constant	96,485 [C/mol]	[22]
Universal gas constant (R_u)	8.314 [J/mol.K]	[35]
Specific surface area of the catalyst layer (A_s)	1 x 10^5 [1/m]	[27]
Pt loading on the catalyst layer (m_{Pt})	4mgPt/cm^2	Assumed
Conductivity of membrane (s_{mem})	σ_m = 7.3 exp(1268(1/298 - 1/T)) [S/m]	[33]
Temperature (T)	353 K	Assumed
Mass fraction of Oxygen in cathode inlet	0.21	Assumed

Summary of parameters used for DMFC computational model.